



Microstructure of NiTi superelastic alloy manufactured by selective laser melting

Emmanuel Nigito, Franck Diemer, S. Husson, S.F. Ou, M.H. Tsai, Farhad Rezai-Aria

► To cite this version:

Emmanuel Nigito, Franck Diemer, S. Husson, S.F. Ou, M.H. Tsai, et al.. Microstructure of NiTi superelastic alloy manufactured by selective laser melting. Materials Letters, 2022, 324, pp.132665. 10.1016/j.matlet.2022.132665 . hal-03713072

HAL Id: hal-03713072

<https://imt-mines-albi.hal.science/hal-03713072>

Submitted on 5 Dec 2022

HAL is a multi-disciplinary open access archive for the deposit and dissemination of scientific research documents, whether they are published or not. The documents may come from teaching and research institutions in France or abroad, or from public or private research centers.

L'archive ouverte pluridisciplinaire **HAL**, est destinée au dépôt et à la diffusion de documents scientifiques de niveau recherche, publiés ou non, émanant des établissements d'enseignement et de recherche français ou étrangers, des laboratoires publics ou privés.

Microstructure of NiTi superelastic alloy manufactured by selective laser melting

E. Nigito^a, F. Diemer^{a,b}, S. Husson^c, S.F. Ou^d, M.H. Tsai^d, F. Rézai-Aria^{a,*}

^a Institut Clément-Ader, Université de Toulouse, CNRS, IMT Mines Albi, INSA, UPS, ISAE-SUPAERO, Campus Jarlard, 81013 Albi CT cedex 09, France

^b Faculté de Chirurgie Dentaire, 3 allée des maraîchers 31000 Toulouse, France

^c Metal Industries Research & Development Centre, Kaohsiung 807, Taiwan

^d Department of Mold and Die Engineering, National Kaohsiung University of Science and Technology, Kaohsiung 807, Taiwan

A B S T R A C T

Nitinol is used in dental tools for its superelasticity, shape memory and biocompatibility. Selective laser melting (SLM) on a powder bed is a potential process for manufacturing such as dental tools. Microstructural studies are conducted on NiTi-SLM using a parallel strip strategy and 90° laser beam rotation. The multi-scale (nano-, micro- and mesoscopic) microstructure is revealed. Similar “cast” type microstructure features are found. The SLM melt is casted in a “micro-mold”. Fine micro-grains with random crystallographic orientation are formed near the mold walls and served as seeds for the rapid growth of columnar dendritic grains along the $\langle 001 \rangle$ direction with epitaxial crystallographic relationships. The growth of the columnar grains curves towards the center of the “micro-mold”, coinciding with the center of the laser beam. It is proposed that SLM processing resembles “Metallic Self Micro-Mold Casting” (MS μ MC) and/or “Self Micro-Molding” (S2M).

1. Introduction

NiTi (Nitinol) alloys exhibit superelastic behavior and shape memory capabilities [1]. Due to good corrosion resistance, biocompatibility and low modulus of elasticity, they are candidates for dental tooling [1]. However, their high elastic spring-back, stress-induced phase transformation and the formation of burrs during machining and forming make their manufacturing very difficult [2]. Powder bed selective laser melting (SLM) has great potential to manufacture complex parts and therefore, is a promising process to manufacture NiTi tools. The effects of main SLM parameters (power, laser scanning speed, hatching, etc.) on microstructure, mechanical properties or phase transformation are already reported [3–4], but limited number of papers deals with microstructure/solidification resulting from extremely rapid “heating/melting” and “solidification/cooling” rates [5]. Present contribution deals with NiTi SLM microstructures according to solidification perspective.

2. Material and experimental procedures

A Ni_{50.63}Ti_{49.37} powder (Plasma AtomisationTM) with a very spherical shape, few satellites and a size distribution between 22 and 48 μ m

($\pm 1 \mu$ m) was purchased from AP&C Company (Canada). SEM examinations (FEI Nova Nano SEM 450 FEG) of the powder revealed a micro-cellular and dendritic microstructure. These features are specific to powder metallurgy roots, due to a rapid solidification.

SLM-125^{HL} machine with infrared laser (400 W, Nd-YAG fiber, $\lambda = 1075$ nm, $d \approx 85 \mu$ m) and a silicone coater is used. 5 mm side cubes (supports of 5 mm high) are produced similarly to [6] with a parallel stripe strategy (laser power 250 W, scan speed 1250 mm.s⁻¹, layer thickness 30 μ m, hatching 120 μ m, laser rotation $\theta = 90^\circ$ and heated TA6V plate (200 °C)), Fig. 1a. The cubes make an angle $\alpha = 30^\circ$ with the coater axis (Fig. 1b).

The “as-fabricated” cubes are sectioned, polished and etched (10–60 s) with a solution of 15 mL HNO₃, 5 mL HF and 35 mL HCl. EBSD investigations are conducted in a JEOL JSM-7100TTLS LV field emission SEM equipped with an Aztec Advanced Nordlys Nano EBSD detector.

3. Results & discussions

SEM observations (Fig. 2) along the XY (a-b-c) and XZ (d-e-f-g-h) plans show that NiTi exhibits a complex multi-scale microstructure with “square patch features” (sides $\approx 120 \mu$ m, Fig. 2.a) due to the fabrication strategy ($h = 120 \mu$ m; $\theta = 90^\circ$). Two features are observed in the XY

* Corresponding author.

E-mail address: farhad.rezai-aria@orange.fr (F. Rézai-Aria).

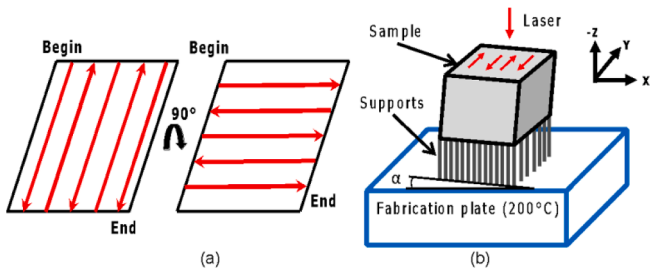


Fig. 1. Schematic of manufacturing with “stripe” strategy and 90° rotation between two consecutive layers (a), sample position on fabrication plate (b).

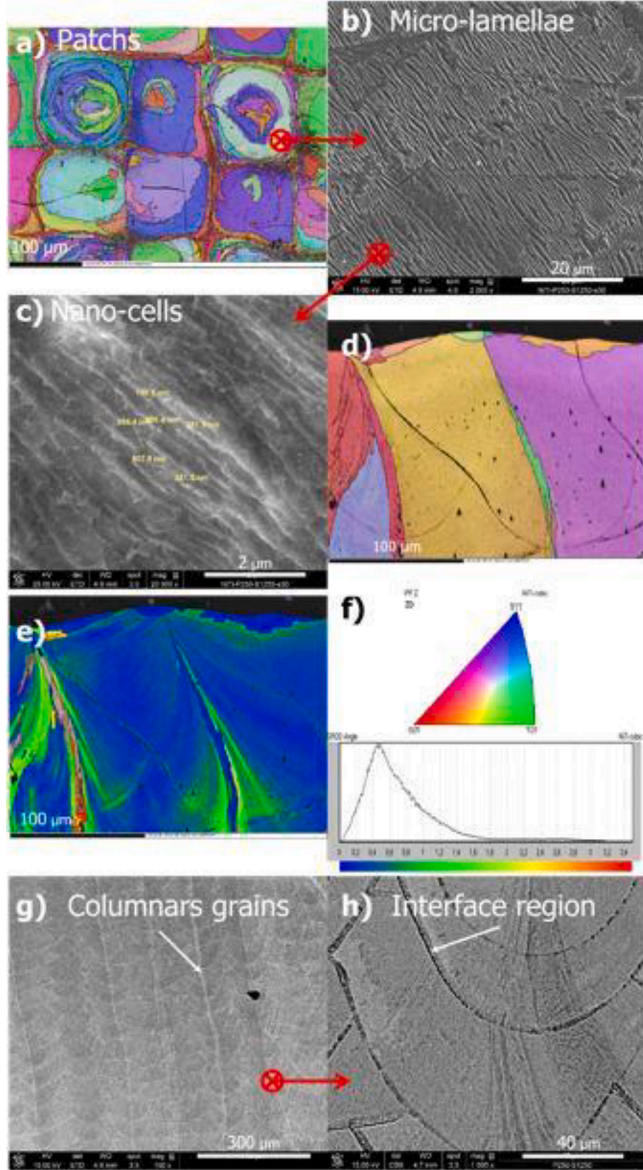


Fig. 2. SEM images of NiTi multi-scale microstructure. Progressive magnification of XY and XZ plans are respectively presented in a-b-c and d-e-f-g-h.

plan. First, “circular” grains (diameters $\approx 100 \mu\text{m}$) within patches oriented mainly along the $\langle 111 \rangle$ and $\langle 101 \rangle$ crystallographic directions. Secondly, elongated grains (width $\approx 5 \mu\text{m}$; length $\approx 100 \mu\text{m}$) oriented mainly along $\langle 001 \rangle$ crystallographic direction and surrounding the patches. At higher magnification, Fig. 2.b, long micro-lamellae

(length $\approx 20 \mu\text{m}$; width $\approx 500 \text{ nm}$) are visible within the patches (white color). Examinations of the inter-lamellar regions (Fig. 2.c) reveal square-like nano-cellular microstructures of about few hundred nanometers sides. The micro-lamellae can be considered as primary dendritic arms and the nano-cells as secondary dendritic arms.

Fig. 2 (d-f) shows XZ plan feature of the last solidified layer/micro-bath. It has a depth of $200 \mu\text{m}$ (about 7 layers of powder) and a diameter at the surface of about twice the laser spot diameter. Each layer is thus rapidly heated, melted and then rapidly cooled for about 7 times. The EBSD color images show the formation of 3 kinds of grains. Firstly, long vertical columnar grains in the center of the micro-bath/micro-mold, with the main axis following $\langle 001 \rangle$ and $\langle 101 \rangle$ orientations, almost parallel to the laser beam. The orientations $\langle 001 \rangle$ and $\langle 101 \rangle$ in the XZ plan coincide with the $\langle 001 \rangle$ direction in the XY plan. Secondly, preferentially $\langle 001 \rangle$ oriented grains are formed on either side of the columnar grains, represented here by alternating purple and orange grains. Like a “mirror”, the grains grow on either side of the laser spot during the forward and backward movement of the laser track. Thirdly, small grains, never seen before, are solidified on the upper surface of the micro-bath. Strong convection/radiation heat exchanges at the free surface of the melt bath with the “inert gas” flow in the fabrication chamber, enhanced by the generated plasma, could form these small grains which are re-melted during the next laser exposure and are therefore only visible on the last fabricated layer.

The GROD analysis, Fig. 2 (e-f), shows very small distortions inside grains developed from the melt/mold interface, “solid wall”, towards the center of the mold and bend towards the Z-axis (upper surface of the melt pool). These distortions can be seen as evidence of the formation of the aforementioned micro-lamellae. It should be noted that the micro-lamellae are not visible on the EBSD IPF map along the XY and XZ plans. It can be assumed that the micro-lamellae are sub-grains with very small misorientations ($\approx 1^\circ$) and therefore not identifiable by conventional IPF mapping.

The cross-section along the XZ plan, Fig. 2 (g-h), shows the interface between two successive melt pools. As conventional foundry, different granular microstructures can be observed in micro-mold. Solidification essentially starts from the “melt pool walls” (1st initial region), develops over a certain distance (2nd intermediate region) and ends in the center of the mold/micro-melt pool (3rd final region).

In SLM, the previously melted layers serve as walls of the micro-mold for the melt and act as heat extractors from the liquid. Near the wall, the heat flow is locally almost perpendicular to the surface. However, due to thermally activated reactions between the liquid and the solid (wall) which is heated below the melting temperature, the dissolution and “washing” of the micro-mold wall surface disrupts the liquid/solid interface as in conventional casting [7]. As a result, the micro-mold surface becomes self-roughening. It is reported that the heat “contact resistance” between the liquid and the solid depends on the roughness of the mold surface [8]. Fine grains or equiaxed cells (Fig. 2.h) are formed near the mold wall and constitute the “child cast” zone. They are randomly oriented in all crystallographic direction, probably due to the self-roughening of the wall surface, which randomly directs the heat extraction vectors.

Assuming that the micro-molds have a parabolic shape (2D cross-section, XZ plan), the columnar grains (Fig. 2.g) grow from micro-mold wall along the $\langle 001 \rangle$ direction. However, due to upward thermal gradients and Marangoni effects, the direction of heat flows converges progressively from the mold wall (lower temperature) towards the center and top of the micro-mold (melt free surface). Solidification follows these heat directions and generates columnar curved grains. This “necessary grain curvature” deforms the atomic planes and cells and generate internal stresses and strains.

In NiTi, as in many alloys with a body-centered cubic lattice, the grains solidify preferentially along $\langle 001 \rangle$ direction, which is commonly referred to as the “natural direction” of solidification. As can be seen in Fig. 2 (g-h), in the bulk of the sample, columnar grains near the center of

the melt solidify from the previous layers. These columnar grains are separated by very fine cellular grains, which maintain the same natural direction of solidification.

At the solidification front, mushy zones form and lead to local micro-segregation by rejection and/or diffusion of Ni and Ti elements on a microscopic scale (micro-lamellae), as in conventional casting. Active exchange of elements can disrupt the solidification front. Wetting phenomenon at grains boundaries [9] could explain these phenomenon of micro-segregation, but results are not enough detailed to conclude it. Observations at higher magnification (microstructure, phases), localized at grains boundaries could allow to have better understanding of solidification and wetting phenomenon on these specific microstructural sites.

SLM is similar to “micro-casting” in “metallic micro-mold”. The micro-volume of alloy consists in several solidified layers and the last layer of spread powder, which is rapidly heated and melted for a short period of time, then rapidly cooled and solidified. In micro-casting, solidification is governed by similar physical phenomena (nucleation and “micro-grain” growth mechanisms) as in conventional die-casting. SLM processing can be considered as “Metallic Self Micro-Mold Casting” (MSuMC) and/or “Self Micro-Molding” (S2M).

4. Conclusions

- SLM processing is considered as “Metallic Self Micro-Mold Casting” (MSuMC) and/or “Self Micro-Molding” (S2M).
- SLM NiTi exhibits complex multi-scale microstructures with patches, micro-lamellae and nano-cells.
- Solidification front basically starts from “micro-mold wall” towards center of melt pool along the heat extraction directions.
- EBSD reveals crystallographic texturing of grains respectively along $\langle 001 \rangle$ direction at the center of laser spot and along $\langle 101 \rangle$ and $\langle 111 \rangle$ directions between the wall and the center of micro-mold.
- Columnar grains grow along the $\langle 001 \rangle$ crystallographic direction (natural direction of solidification) and preserved an epitaxial relationship with the grains at the surface of the micro-mold.
- Thermal convection and radiation play important role in solidification during SLM manufacturing.

CRedit authorship contribution statement

E. Nigito: Conceptualization, Investigation, Data curation, Writing –

review & editing, Visualization. **F. Diemer:** Conceptualization, Resources, Writing – review & editing, Supervision. **S. Husson:** Conceptualization, Resources. **S.F. Ou:** Conceptualization, Resources. **M.H. Tsai:** Conceptualization, Resources. **F. Rézai-Aria:** Conceptualization, Resources, Data curation, Writing – review & editing, Supervision, Project administration, Funding acquisition.

Declaration of Competing Interest

The authors declare that they have no known competing financial interests or personal relationships that could have appeared to influence the work reported in this paper.

Acknowledgments

Joint financial support from French Occitanie Region and IMT Mines Albi are acknowledged. Micro-analysis Raymond Castaing Center, Toulouse is acknowledged for EBSD investigations.

References

- [1] H. Walia, W.A. Brantley, H. Gerstein, An initial investigation of the bending and torsional properties of nitinol root canal files, *J. Endod* 14 (7) (1988) 346–351.
- [2] M.H. Elahinia, M. Hashemi, M. Tabesh, S.B. Bhaduri, Manufacturing and processing of NiTi implants: A review, *Prog. Mater. Sci.* 57 (5) (2012) 911–946.
- [3] S. Saeedi, A.S. Turabi, M. Taheri Andani, C. Haberland, H. Karaca, M. Elahinia, The influence of heat treatment on the thermomechanical response of Ni-rich NiTi alloys manufactured by selective laser melting, *J. Alloys Compounds* 677 (2016) 204–210.
- [4] M. Speirs, X. Wang, S. Van Baelen, A. Ahadi, S. Dadbakhsh, J.-P. Kruth, J. Van Humbeeck, On the transformation behavior of NiTi shape-memory alloy produced by SLM, *Shape Mem. Superelasticity* 2 (4) (2016) 310–316.
- [5] L. Qian, J. Mei, J. Liang, X. Wu, Influence of position and laser power on thermal history and microstructure of direct laser fabricated Ti–6Al–4V samples, *Mater. Sci. Technol.* 21 (5) (2005) 597–605.
- [6] M. Elahinia, N. Shayesteh Moghaddam, M. Taheri Andani, A. Amerinatanzi, B. A. Bimber, R.F. Hamilton, Fabrication of NiTi through additive manufacturing: A review, *Prog. Mater. Sci.* 83 (2016) 630–663.
- [7] M. Salem, S. Le Roux, G. Dour, P. Lamesle, K. Choquet, F. Rézai-Aria, Effect of aluminizing and oxidation on the thermal fatigue damage of hot work tool steels for high pressure die casting applications, *Int. J. Fatigue* 119 (2019) 126–138.
- [8] A. Hamasaid, G. Dour, T. Loulou, M.S. Dargusch, A predictive model for the evolution of the thermal conductance at the casting–die interfaces in high pressure die casting, *Int. J. Therm. Sci.* 49 (2) (2010) 365–372.
- [9] B.B. Straumal, A.S. Gornakova, Y.O. Kucheev, B. Baretzky, A.N. Nekrasov, Grain Boundary Wetting by a Second Solid Phase in the Zr–Nb Alloys, *J. of Materi Eng and Perform* 21 (5) (2012) 721–724.